IIETA International Information and Engineering Technology Association
Advancing the World of Information and Engineering

Journal Européen des Systèmes Automatisés
Vol. 59, No. 2, February, 2026, pp. 303-314
Journal homepage: http://iieta.org/journals/jesa

Performance Evaluation of PID, Fuzzy, and ANFIS Controllers for DC–DC Buck Converters under Reference and Load Disturbances

Abdulrahman Kareem[1*], Ayad Al-Dujail[1], Amjad Jaleel Humaidi[2]

[1] Electrical Engineering Technical College, Middle Technical University, Baghdad 10098, Iraq
[2] College of Artificial Intelligence Engineering, University of Technology, Baghdad 10066, Iraq

Corresponding Author Email: amjad.j.humaidi@uotechnology.edu.iq

https://doi.org/10.18280/jesa.590202

Received: 10 December 2025
Revised: 11 February 2026
Accepted: 20 February 2026
Available online: 28 February 2026

Keywords:
DC-DC buck converters, proportional-integral-derivative controller, Fuzzy Logic Controller, adaptive neuro-fuzzy inference system, robustness, dynamic performance

ABSTRACT

A DC-DC buck converter is a step-down power supply commonly used in embedded systems and renewable energy applications due to its high efficiency, compact design, and accurate output-voltage regulation. The main challenge is selecting suitable parameters and structural configurations for each controller to achieve robust, fast, and low-ripple regulation across various operating conditions. This paper provides a comparative analysis of three control strategies: a conventional proportional-integral-derivative (PID) controller, a Fuzzy Logic Controller (FLC), and an adaptive neuro-fuzzy inference system (ANFIS)-based neuro-fuzzy controller. These controllers are used to regulate a buck converter. The converter's mathematical model is initially developed, followed by the design and implementation steps for the PID, FLC, and ANFIS. MATLAB/Simulink tests verify the controllers' proper operation under changes in the reference and load disturbances. The comparison highlights two key criteria: robustness and dynamic output voltage performance. Results show that the ANFIS best adapts to parameter variations, exhibiting the lowest overshoot and the fastest settling time. The FLC performs well, with quick tracking and minimal residual oscillations. Conversely, the PID controller results in larger transient deviations and slower damping.

1. INTRODUCTION

DC–DC buck converters are commonly used as efficient step-down stages in regulated DC supplies for embedded electronics, telecommunications, point-of-load regulation, automotive auxiliaries, and various power-electronic interfaces. Due to their switched nonlinear dynamics, sudden load changes, and component tolerances, buck converters can display overshoot, ripple, and slow recovery if the feedback controller is not designed to ensure proper damping and disturbance rejection. Thus, achieving fast transient response with low steady-state error and minimal voltage/current ripple remains a key control goal for buck converters, especially during reference changes and load disturbances [1, 2].

Conventional proportional-integral-derivative (PID) control remains popular because of its simple structure and ease of real-time implementation. However, fixed PID gains can reduce performance when operating conditions change or unmodeled dynamics and parameter uncertainties occur. To address these issues, intelligent control strategies such as Fuzzy Logic Controller (FLC) and adaptive neuro-fuzzy inference systems (ANFIS)-based controllers are increasingly studied for power converters to enhance robustness and transient response.

A brief review of control techniques in the literature is provided below. Yusoff et al. [3] compared FLC and PID with other control methods for a DC-DC buck converter. They indicated that FLC achieved reduced settling time and less overshoot at operating points. The paper highlights the strong, dynamic performance of FLC, which demonstrates tight voltage regulation. Swathy et al. [4] evaluated an FLC for closed-loop regulation of a DC–DC buck converter and benchmarked it against conventional linear controllers such as PID. The study reports that FLC yields improved transient behavior, characterized by reduced overshoot and shorter settling time, while maintaining tighter output-voltage regulation and stronger robustness to operating-point and load variations. Fudoli et al [5] compared a classical Proportional-Integral (PI) controller with a fuzzy-logic PI scheme for buck-converter output-voltage regulation. Using step and load-disturbance scenarios, they assessed overshoot and settling time. The fuzzy PI consistently delivered shorter settling time and reduced overshoot, implying superior closed-loop stability and robustness compared to the classical PI. Guiza et al. [6] proposed a Takagi–Sugeno fuzzy tracking controller for a DC–DC buck converter using an exact T–S fuzzy model and virtual desired variables. Controller gains were derived via LMI conditions, yielding faster rise and settling times and zero overshoot compared to a baseline PI regulator. Bhat et al. [7] compared PI and fuzzy-logic control for a DC-DC buck converter. They report that fuzzy control achieves faster transient response with minimal overshoot and reduced voltage and current ripple, providing tighter output-voltage regulation than conventional PI across operating conditions.

Martínez et al. [8] proposed an advanced fuzzy inference–based control scheme for synchronous buck converters in renewable-energy applications. By combining adaptive, feedforward, and multivariable fuzzy reasoning, the controller improves voltage regulation and closed-loop stability, achieving faster settling, lower overshoot, and smaller steady-state error than a conventional PID under load and input-voltage variations. Shaikh et al. [9] introduced hybrid ANFIS–PID control structures for buck converters, including a novel product-type hybrid that multiplies ANFIS and PID outputs. Comparative results against classical PID indicate improved tracking quality, with reduced steady-state error and marginal overshoot reduction, alongside a higher peak efficiency (96.5%) across load conditions. Shabaninia et al. [10] developed a neuro-fuzzy PD controller for a Pulse-Width Modulation (PWM) buck converter and, through simulation (using ANFIS-based), demonstrated strong performance with improved transients (lower overshoot) and shorter settling times compared to standard fuzzy PID/PD versions. Nejad et al. [11] developed an ANFIS-based controller for a DC-DC buck converter. They demonstrated strong noise tracking, supply, and load response, and compared it with fuzzy-PID and Particle Swarm Optimization (PSO)-PID, which had faster responses and higher disturbance rejection.

This paper addresses the above gap by providing a unified simulation-based benchmark of three controllers-PID, FLC, and an ANFIS-based neuro-fuzzy controller-applied to the same buck-converter plant with the same operating constraints and switching conditions. The controllers are evaluated under strictly identical reference-step and load-disturbance scenarios. Performance is quantified using consistent metrics, including rise time, settling time, overshoot/undershoot, steady-state error, output-voltage ripple, inductor-current ripple, and disturbance rejection.

The main contributions of this work are summarized as follows:

1) A standardized benchmarking framework for PID, FLC, and ANFIS-based neuro-fuzzy control applied to the same DC–DC buck converter under identical operating constraints and disturbance scenarios (constant-reference regulation, reference-step change, and step load disturbance), enabling direct quantitative comparison.
2) A documented neuro-fuzzy controller development process in which the ANFIS model is initialized from the designed FLC rule base; training input–output pairs are generated from the FLC mapping (e and de to duty-cycle command), and ANFIS training refines the membership functions and consequent parameters, with the resulting changes linked to the control surface and closed-loop performance.
3) A comprehensive evaluation protocol that reports output-voltage tracking, error dynamics, and duty-cycle behavior using unified time-domain and ripple-related performance indices, providing a consistent basis to assess transient response, steady-state accuracy, ripple, and disturbance rejection.

2. MATHEMATICAL MODEL OF BUCK CONVERTER

Figure 1 illustrates the equivalent circuit of a Buck converter, a step-down DC-DC converter that reduces the input voltage to a regulated output voltage. The circuit includes an input voltage source, a controlled semiconductor switch, a diode, an inductor, an output filter capacitor, and a load resistance. Filter capacitor C, and a load resistance R.

The inductor L stores energy during the switch-on period and releases it during the OFF period, ensuring continuous current flow. The capacitor C filters the output voltage, reducing ripple and maintaining a stable DC level at the load. The load resistor R represents the electrical demand connected to the converter's output. The switch M is operated with a duty cycle d, which directly determines the voltage conversion ratio. The diode D provides a freewheeling path for the inductor current when the switch is OFF, preventing abrupt current interruption.

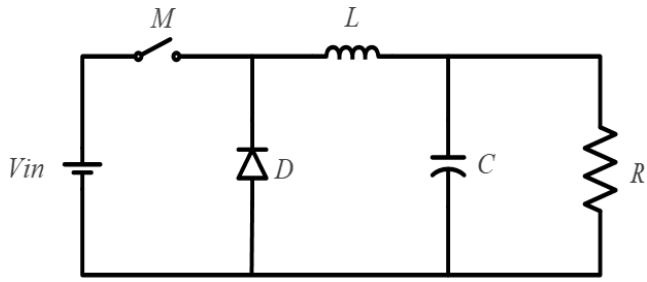

Figure 1. DC-DC buck converter schematic diagram

The circuit's dynamic behavior can be represented in state-space form, with the inductor current as the state variable. Li and the output voltage V_o chosen as the state variables. Applying Kirchhoff's Voltage Law (KVL), the following equations are obtained.

$$\dot{x}_1 = \frac{d}{L}V_{in} - \frac{1}{L}x_2 \tag{1}$$

$$\dot{x}_2 = \frac{1}{C}x_1 - \frac{1}{RC}x_2 \tag{2}$$

In matrix form, with V_{in} considered as the input, the system can be expressed as:

$$\dot{x} = \begin{bmatrix} 0 & -\frac{1}{L} \\ \frac{1}{C} & -\frac{1}{RC} \end{bmatrix} x + \begin{bmatrix} \frac{d}{L} \\ 0 \end{bmatrix} V_{in}, \qquad y = [0 \quad 1]x. \tag{3}$$

By controlling the duty cycle d, the relationship between the input and output voltages is given by

$$V_o = d \cdot V_{in} \quad \Rightarrow \quad d = \frac{V_o}{V_{in}} \tag{4}$$

Using Table 1, we obtain the following numerical values for the matrices:

$$A = \begin{bmatrix} 0 & -\frac{1}{0.2} \\ \frac{1}{0.001} & -\frac{1}{5\times 0.001} \end{bmatrix} = \begin{bmatrix} 0 & -5 \\ 1000 & -200 \end{bmatrix} \tag{5}$$

$$B = \begin{bmatrix} 0.625 \\ \overline{0.2} \\ 0 \end{bmatrix} = \begin{bmatrix} 3.125 \\ \\ 0 \end{bmatrix}, C = [0 \quad 1]. \tag{6}$$

The final state–space model is:

$$\dot{x} = \begin{bmatrix} 0 & -5 \\ 1000 & -200 \end{bmatrix} x + 3.1250 Vin \tag{7}$$

$$y = [0 \quad 1] x \tag{8}$$

Table 1. The parameters of the DC–DC converter are given by the study [12]

Parameter Description	Value
Duty Cycle (d)	0.625
Inductor (L)	0.2 H
Capacitor (C)	1 mF
Load Resistance (R)	5 Ω
Switching Frequency (fs)	20 kHz

3. PROPOSED CONTROL STRATEGIES

In this section, three control paradigms for regulating the buck DC–DC converter's output voltage is considered: a conventional PID controller, a classical FLC, and a neuro-fuzzy controller (ANFIS). The PID controller is characterized by its proportional, integral, and derivative gains, which are tuned to achieve the desired closed-loop dynamics. The FLC is defined by its linguistic variables, membership functions, and rule base. The ANFIS employs an ANFIS-like structure that combines fuzzy inference with neural network learning, enabling data-driven parameter adaptation.

3.1 Proportional-integral-derivative-based controller design

To ensure a principled and reproducible tuning procedure, the PID gains were initialized using the averaged small-signal model of the buck converter operating in continuous-conduction mode (CCM), and subsequently verified through time-domain tests. By linearizing the averaged state-space equations around the nominal operating point, the duty-cycle–to–output-voltage transfer function is obtained as

$$Gvd(s) = \frac{Vin}{\left(L C s^2 + \left(\frac{L}{R} \right) s + 1 \right)} \tag{9}$$

which adequately represents the dominant output-filter dynamics within the frequency range of interest.

A frequency-domain loop-shaping strategy was employed to determine the controller parameters. The target closed-loop bandwidth was deliberately selected to be well below the PWM switching frequency ($fs = 20\,kHz$) to preserve the validity of the averaged-model approximation and to mitigate high-frequency duty-cycle chatter. The adopted compensator has the standard PID form:

$$C(s) = Kp + \frac{Ki}{s} + Kd\, s. \tag{10}$$

The placement of controller zeros was guided by the plant dynamics: integral action provides low-frequency gain to eliminate steady-state regulation error, whereas the derivative term introduces phase lead to enhance damping and transient performance. In particular, the controller zero frequencies are $\omega zi = Ki/Kp$ and $\omega zd = Kp/Kd$, which were positioned to support robust tracking while maintaining adequate phase characteristics near the unity-gain crossover.

Using the final gains ($Kp = 0.15$, $Ki = 10$, $Kd = 0.005$), the open-loop transfer function $L(s) = C(s)\,Gvd(s)$ exhibits a unity-gain crossover frequency of $\omega c \approx 34 rad/s$ and an estimated phase margin of approximately 80°, indicating a robust stability buffer against modelling uncertainty and operating-point variations. Moreover, the gain margin is effectively large because the open-loop phase does not approach $-180°$ over the frequency range relevant to the designed bandwidth. Following this model-based initialisation, limited time-domain simulations under reference-step and load-step disturbances were performed only as a final validation stage, ensuring that transient indices and ripple-related performance metrics satisfy the study's requirements without relying on trial-and-error as the primary design method.

The closed-loop PID regulation structure adopted in this study is depicted in Figure 2.

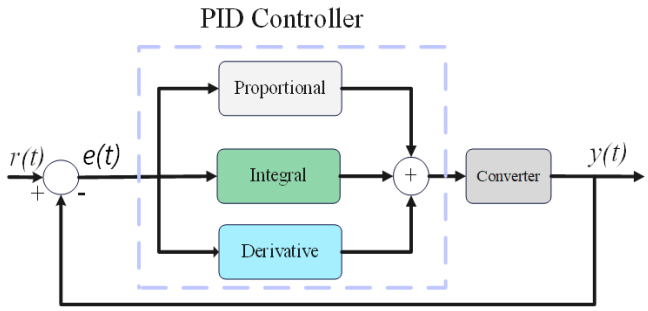

Figure 2. Proportional-integral-derivative (PID) controller

3.2 Fuzzy Logic Controller-based controller design

The FLC regulates the buck-converter output by mapping the instantaneous voltage error and its rate of change to a duty-cycle command. The input variables are defined as

$$e(t) = vref(t) - vo(t), e'(t) = \frac{de(t)}{dt} \tag{11}$$

where, e represents the tracking error and $e`$ provides derivative-sensitive information for damping.

The overall FLC-based closed-loop regulation scheme is illustrated in Figure 3.

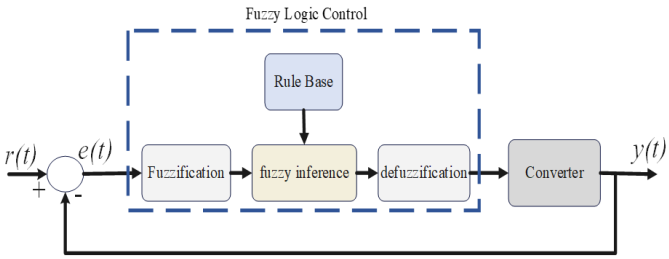

Figure 3. Fuzzy Logic Controller (FLC)

Universes of discourse: The input universes are selected to cover the maximum expected excursions under the standardized reference-step and load-disturbance scenarios used in this paper, with an additional safety margin to prevent saturation. Accordingly, the error universe is set to $e \in [-5, 5]$, which safely covers the largest anticipated deviation from the setpoint (including margin), while the change-of-error universe is set to $e` \in [-10, 10]$, chosen to encompass the maximum expected error slope during the transient (based on the controller update interval and the observed worst-case response). These ranges provide high sensitivity near the setpoint and sufficient coverage under large disturbances.

The implemented FIS configuration in the MATLAB Fuzzy Designer is shown in Figure 4. Each input is partitioned into nine Gaussian membership functions (NB, NM, NS, NVS, Z, PVS, PS, PM, PB), as shown in Figures 5 and 6. Nine membership functions are adopted as a compromise between control resolution and rule-base complexity: the "very small" regions (NVS/PVS) around zero enable fine corrective action near regulation to reduce ripple, while the additional granularity away from zero improves transient damping and overshoot control. Gaussian membership functions are selected because their smooth overlap yields a smooth duty-cycle command and avoids abrupt control variations.

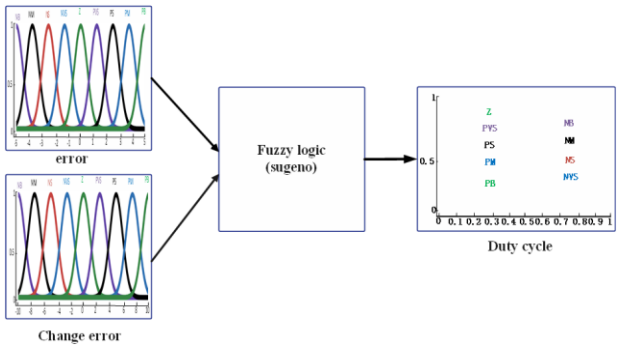

Figure 4. Fuzzy designer

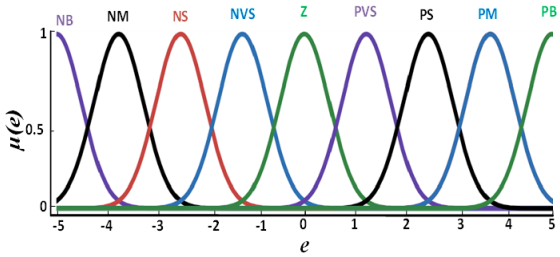

Figure 5. Gaussian membership function of the input variable "e"

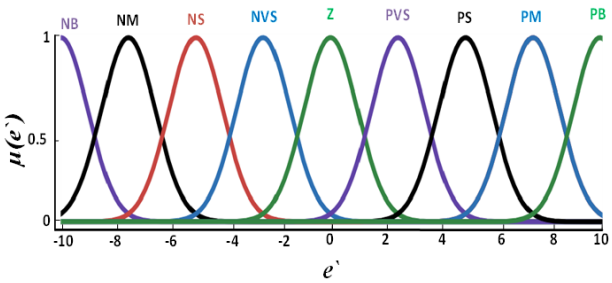

Figure 6. Gaussian membership function of the input variable "$e`$"

The Gaussian membership functions used for the input variables e and e' are presented in Figures 5 and 6, while the output representation is shown in Figure 7.

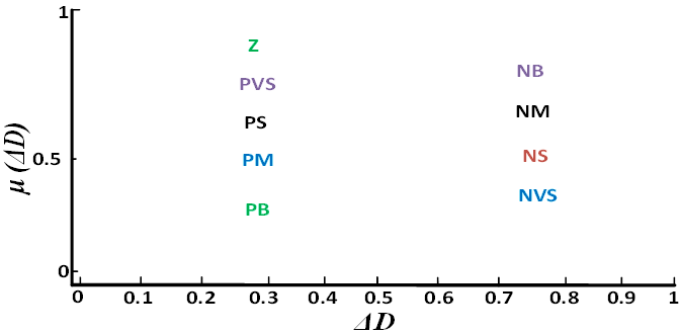

Figure 7. Membership function of the output variable

Table 2. The fuzzy control rules

		e							
		NB	**NM**	**NS**	**NVS**	**Z**	**PVS**	**PS**	**PM**	**PB**
de	**NB**	NB	NB	NB	NM	NM	NS	NVS	PVS	PS
	NM	NB	NB	NM	NM	NS	NS	NVS	PS	PS
	NS	NB	NM	NM	NS	NS	NVS	PVS	PS	PM
	NVS	NM	NM	NS	NVS	NVS	PVS	PS	PM	PM
	Z	NM	NS	NS	NVS	Z	PVS	PS	PM	PB
	PVS	NS	NVS	PVS	PVS	PVS	PS	PM	PM	PB
	PS	NVS	PVS	PS	PS	PS	PM	PM	PB	PB
	PM	PVS	PS	PS	PM	PM	PM	PB	PB	PB
	PB	PS	PS	PM	PM	PB	PB	PB	PB	PB

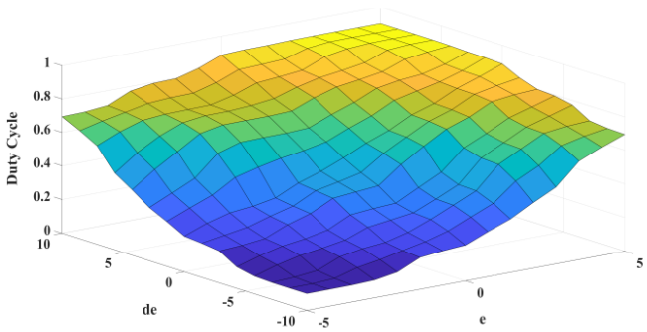

Figure 8. Control surface of Fuzzy Logic Controller (FLC)

Inference and output computation (consistency clarification): The implemented FLC is a zero-order Sugeno (TSK) FIS. The rule base (Table 2) generates singleton consequents for the duty-cycle command D. The firing strength of each rule is computed from the input MF degrees using a standard T-norm (e.g., product or min), and the crisp output is obtained by the Sugeno weighted-average:

$$D = (\Sigma wi \cdot Di)/(\Sigma wi) \quad (12)$$

where, w_i is the firing strength of the i-th rule, and Di is the corresponding singleton consequent. The duty-cycle command is finally limited to a safe operating range $[Dmin, Dmax]$ before driving the PWM stage. The resulting rule surface (Figure 8) is monotonic and derivative-sensitive, providing stronger correction far from the setpoint and gentler action near regulation, which helps reduce overshoot and ripple.

3.3 Adaptive neuro-fuzzy inference system-based controller design

The buck DC–DC converter exhibits nonlinear and switching-dependent dynamics; therefore, intelligent control techniques can provide improved regulation performance compared to fixed-gain classical controllers under varying operating conditions [13]. In this work, a neuro-fuzzy controller is developed using an ANFIS. The ANFIS combines the interpretability of fuzzy rules with data-driven parameter adaptation, enabling an enhanced nonlinear mapping from the error signals to the duty-cycle command [14, 15]. Figure 9 illustrates the ANFIS structure adopted in this study. A first-order Sugeno (TSK) ANFIS is used, with two inputs and one output. The inputs are the voltage tracking error and its change:

$$e(t) = vref(t) - vo(t), e'(t) = \frac{de(t)}{dt} \tag{13}$$

And the ANFIS output is the duty-cycle increment ΔD (bounded to the safe range $[Dmin, Dmax]$ before driving the PWM).

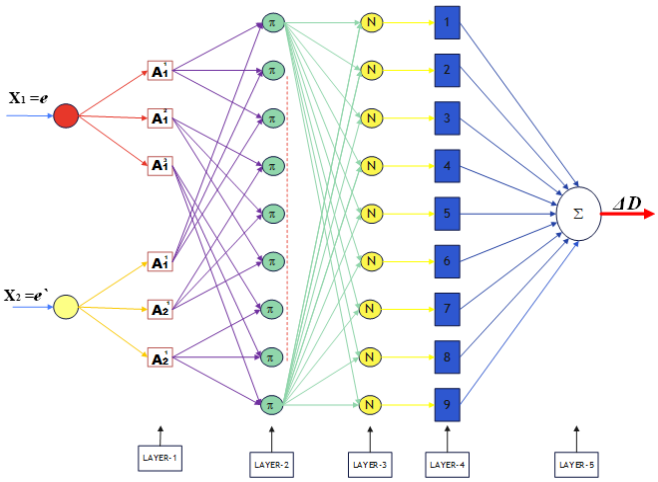

Figure 9. Structure of adaptive neuro-fuzzy inference system (ANFIS)

First-order Sugeno ANFIS rules and layer computations for a first-order Sugeno ANFIS, the i-th rule is expressed as [13]:

If X is A_i and Y is B_i, then

$$f_i = p_i x + q_i y + r_i \tag{14}$$

where, $X \triangleq e$ and Y ≙ e'. The parameters (p_i, q_i, r_i) are the consequent parameters, while A_i and B_i are the premise (input) membership functions (MFs). The overall ANFIS computation can be described layer-by-layer as follows (the input layer is counted separately, hence a six-layer representation including inputs, consistent with Figure 10:

Layer 1 (premise MFs): Each node computes the MF grade of the inputs:

$$O_{1,i} = \mu_{A_i}(x), \quad i = 1,2,\ldots,M \tag{15}$$

$$O_{2,i} = \mu_{B_i}(y), \quad j = 1,2,\ldots,K \tag{16}$$

where, M and K are the numbers of MFs assigned to X and Y, respectively.

Layer 2 (rule firing): Each node computes the firing strength of a rule using a T-norm (product is used here):

$$w_i = \mu_{A_i}(x).\mu_{B_i}(y) i = 1,2,\cdots,5Nr \tag{17}$$

where, Nr is the number of rules.

Layer 3 (normalization): The firing strengths are normalized:

$$\bar{w}i = wi/(\Sigma wi), i = 1,2,\ldots,Nr \tag{18}$$

Layer 4 (rule outputs): Each node computes the weighted rule output:

$$O_{4,i} = \bar{w}i\ fi = \bar{w}i(pi\ X + qi\ Y + ri) \tag{19}$$

Layer 5 (aggregation/output): The final crisp output is obtained by summing all rule contributions:

$$\Delta D = \Sigma \bar{w} i fi = (\Sigma wi fi)/(\Sigma wi) \tag{20}$$

Unlike Mamdani FIS, a first-order Sugeno ANFIS represents the output through rule consequents (linear functions) rather than output membership functions; therefore, training refines the premise (input MF) parameters and the consequent coefficients.

Training-data generation (N = 100 samples) to avoid a black-box training description, the ANFIS training dataset is generated offline from the baseline FLC mapping (not from closed-loop time-series). Specifically, the defined input universes of discourse are sampled to produce N = 100 input pairs (X_K, Y_K) over the ranges used in the fuzzy design. For each sampled pair, the baseline FLC is evaluated to generate the target output $y_K = \Delta D\_FLC, k$. Hence, the dataset is:

$$(X_K, Y_K) \rightarrow y_K \quad for\ k = 1,\ldots,100. \tag{21}$$

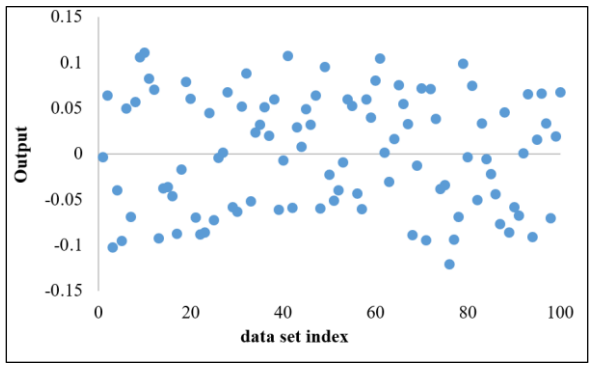

Figure 10. Loading training data into the neuro-fuzzy designer

Figure 10 shows the imported training dataset used within the neuro-fuzzy designer.

Learning algorithm, objective function, and training settings

Training is performed using the standard ANFIS hybrid learning algorithm in MATLAB: in the forward pass, the consequent parameters (p_i, q_i, r_i) are identified via least-squares estimation (LSE), while in the backward pass the premise parameters of the input Gaussian MFs (centers and spreads) are updated via gradient descent/backpropagation to reduce the fitting error [16]. The optimization objective is the mean-squared error (MSE):

$$J = \left(\frac{1}{N}\right)\Sigma k\left(yANFIS, k - yk\right)^2 \tag{22}$$

As shown in Figure 11, the training error converges rapidly within the first iterations and stabilizes by 100 epochs, indicating a consistent fit to the target mapping. The training dataset used for the ANFIS model is provided in the Appendix.

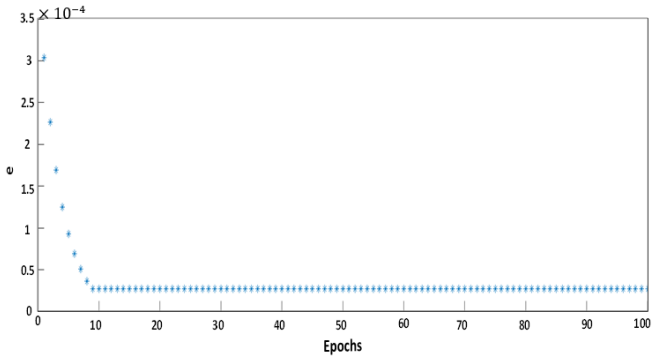

Figure 11. Adaptive neuro-fuzzy inference system (ANFIS) training error (MSE) versus epochs

Figure 12 shows a neural network that explains the structure of the ANFIS model, with two inputs and one output. Each input has a set of membership functions assigned to it, and combining these with the AND operation forms fuzzy rules. For each rule, a value is generated, and these values are summed to produce a final single value.

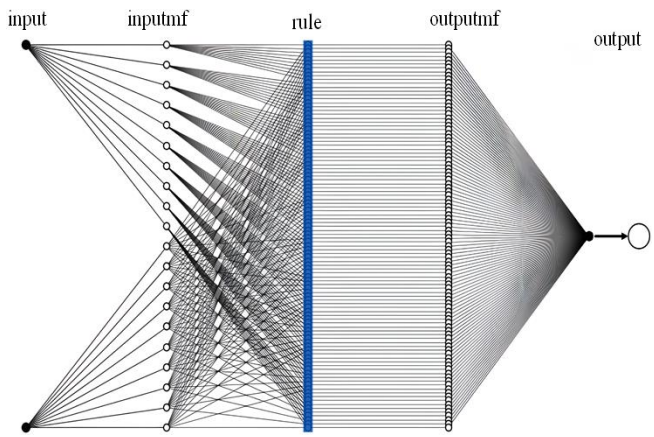

Figure 12. Neural network diagram

Effect of training on MFs and control surface. After training, a new FIS is obtained. The learned ANFIS slightly adjusts the input MF parameters and the consequent coefficients to better approximate the target nonlinear mapping. The resulting trained control surface is shown in Figure 13. Compared with the baseline FLC surface (Figure 8), the trained surface preserves the same global monotonic/derivative-sensitive behavior, while introducing refined nonlinear shaping in specific regions of the (e, e') plane. This adjustment modifies the local slope (effective control gain) of the mapping, which is reflected in the improved transient damping and disturbance recovery reported in the comparative results under identical test scenarios.

Figure 13 shows the ANFIS control surface after learning. Relative to the baseline FLC surface (Figure 9), the ANFIS surface exhibits refined nonlinear shaping (modified local slope) while preserving the global monotonicity and derivative sensitivity.

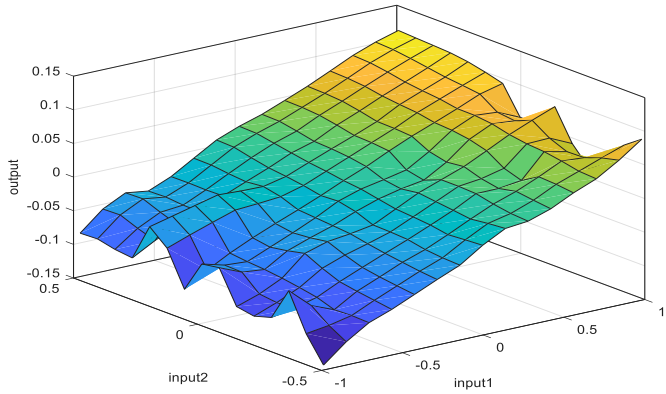

Figure 13. New rules surface after training in adaptive neuro-fuzzy inference system (ANFIS)

4. RESULTS AND DISCUSSION

Table 3 summarizes the experimental configuration used to benchmark the three control paradigms (PID, FLC, and ANFIS). All evaluations were performed on the same buck converter under identical operating conditions (fixed input voltage and identical inductor, capacitor, and load values).

Table 3. The parameters and values for the buck DC-DC converter

Parameter Name	Value
Input voltage	8 Volt
output voltage	5 Volt
Inductor	0.2 H
Capacitor	1 mF
Load resistance	5 Ω
Switching frequency	20 kHz

Figure 14 shows the Simulink model used to implement the FLC and ANFIS for the buck converter. The PID controller is implemented using an analogous structure, with the PID block replacing the FLC/ANFIS block.

4.1 Case-1 (Constant-reference tracking)

In this experiment, a DC-DC buck converter is configured to reduce the output voltage from 8 V to 5 V. Three controllers, namely PID, FLC, and ANFIS, are tested under the same hardware and operating conditions to measure voltage regulation and reference tracking carefully.

Figure 15 shows that the PID controller (solid black) exhibits significant initial overshoot and weakly damped oscillations before reaching the 5 V reference. The FLC (black dotted) provides a quicker response, though it exhibits small residual ripples during the transient interval. Conversely, the ANFIS (red) shows the smallest overshoot and the shortest settling time, approaching the steady-state value smoothly and without oscillation. Therefore, the ANFIS is superior in terms of transient performance and strength compared to the PID and FLC controllers.

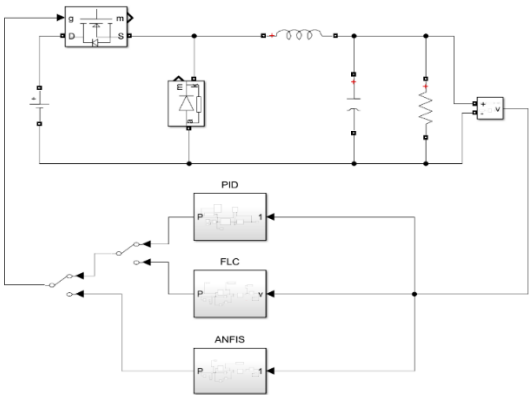

Figure 14. A Simulink model of proportional-integral-derivative (PID) controller, Fuzzy Logic Controller (FLC) and adaptive neuro-fuzzy inference system (ANFIS) for a buck converter

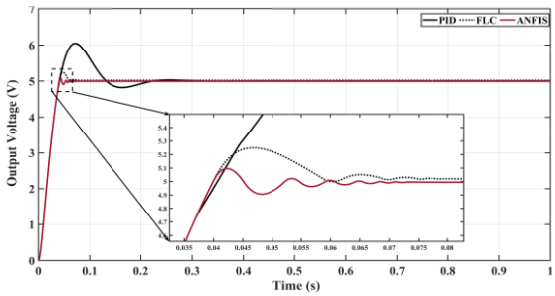

Figure 15. Output voltage of the buck converter for case 1

The corresponding tracking error is shown in Figure 16, while the duty-cycle control signals for PID, FLC, and ANFIS are shown in Figures 17-19, respectively.

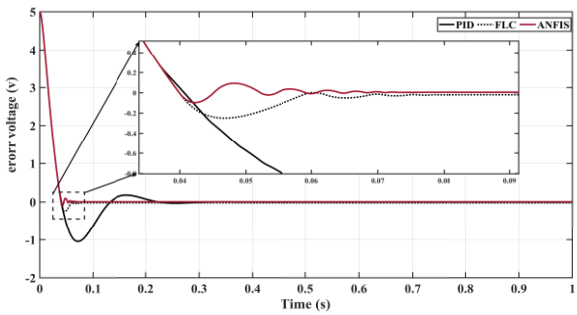

Figure 16. Error of the buck converter for case 1

At the reference step change occurring at $t = 0.5\,s$, as illustrated in Figure 20, similar trends are observed. The PID (solid black) controller shows a large transient deviation and slower recovery, while the FLC (black dotted) responds more rapidly with reduced oscillatory behavior. The ANFIS (red) controller again provides the smoothest transition to the new reference level, with negligible steady-state error and superior disturbance rejection. The tracking error and duty-cycle control signals for PID, FLC, and ANFIS in the reference-step test are presented in Figures 21-24.

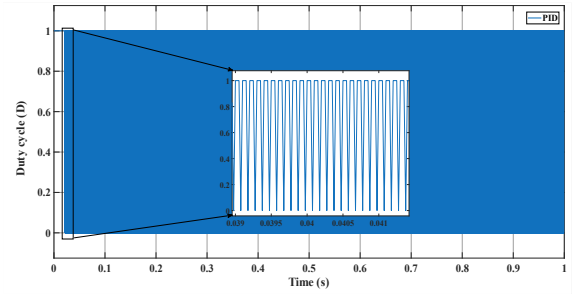

Figure 17. Duty-cycle control signal for proportional-integral-derivative (PID) controller case 1

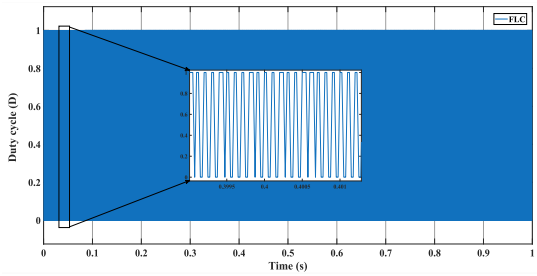

Figure 18. Duty-cycle control signal for Fuzzy Logic Controller (FLC) case 1

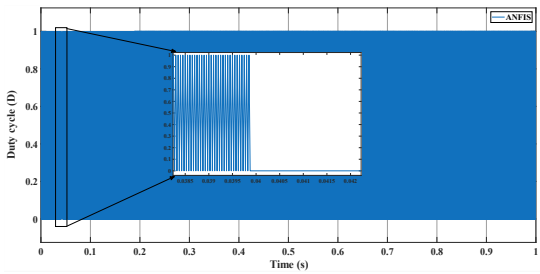

Figure 19. Duty-cycle control signal for adaptive neuro-fuzzy inference system (ANFIS) case 1

4.2 Case-2 (Reference step change test)

To evaluate reference-tracking capability, the DC–DC buck converter's output set-point is stepped from 6 V to 4 V. The dynamic responses of three controllers ,PID, FLC, and ANFIS, are compared under identical conditions to assess transient and steady-state performance.

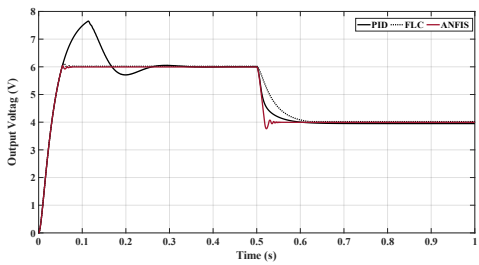

Figure 20. Output voltage of the buck converter for case 2

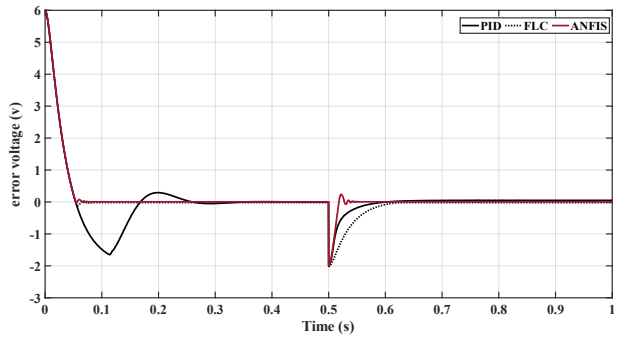

Figure 21. Error of the buck converter for case 2

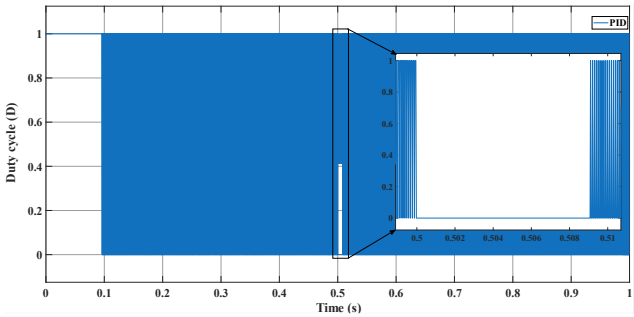

Figure 22. Duty-cycle control signal for proportional-integral-derivative (PID) controller case 2

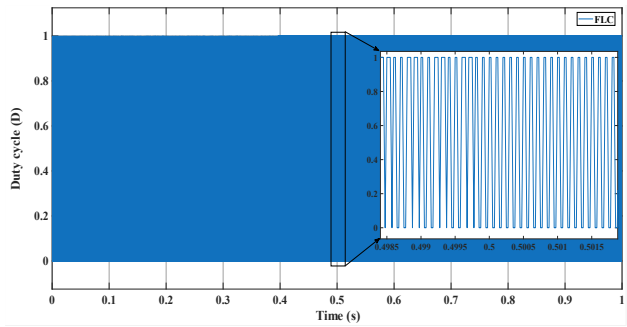

Figure 23. Duty-cycle control signal for Fuzzy Logic Controller (FLC) case 2

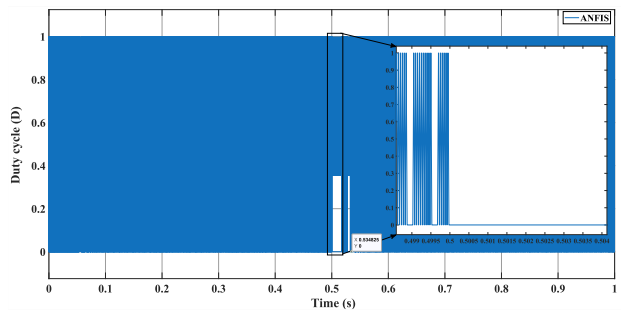

Figure 24. Duty-cycle control signal for adaptive neuro-fuzzy inference system (ANFIS) case 2

4.3 Case-3 (load step disturbance)

To assess robustness against sudden disturbances, a step load change is implemented by reducing the load from 5 Ω to 3 Ω. The closed-loop responses of three controllers- PID, FLC, and ANFIS-are evaluated under identical conditions to measure voltage regulation resilience.

As Figure 25, at t = 0.5 s, during the application of the load perturbation, the PID controller (solid black) exhibits a strong transient with overshoot/undershoot, as well as considerable ringing, before stabilization. The FLC (black dotted) performs better in terms of disturbance rejection, settling faster with fewer oscillations and exhibiting a small overshoot. Conversely, ANFIS (red) shows the least deviation from the 5 V reference, the quickest recovery, and only the slightest residual ripple (as verified in the zoomed inset). In general, ANFIS can be considered the most stable and the most robust to disturbances among the three controllers.

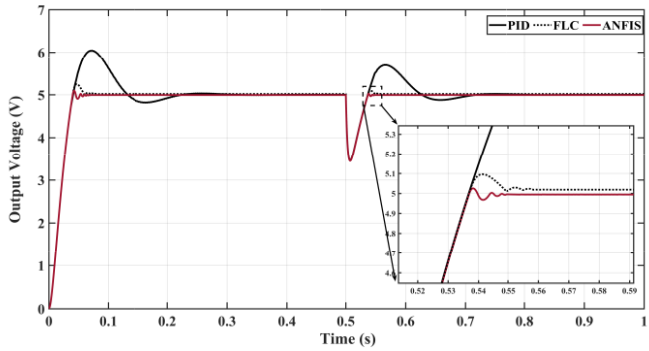

Figure 25. Output voltage of the buck converter for case 3

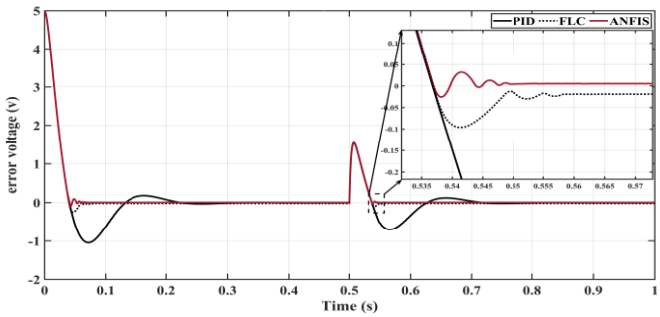

Figure 26. Error of the buck converter for case 3

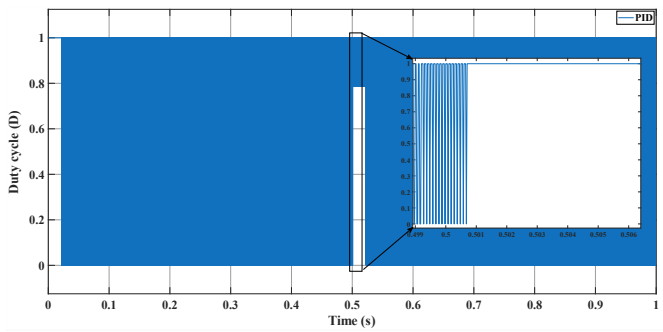

Figure 27. Duty-cycle control signal for proportional-integral-derivative (PID) case 3

Figure 26 presents the corresponding tracking error for case 3 and confirms that the ANFIS controller produces the smallest deviation and the fastest error decay. The duty-cycle control signals for the PID, FLC, and ANFIS controllers in case 3 are shown in Figures 27, 28, and 29, respectively.

A quantitative summary of the transient indices (rise time, settling time, and maximum overshoot) is provided in Table 4. In addition, the error-based performance measures (RMSE, MAE, and ITAE) are summarized in Table 5.

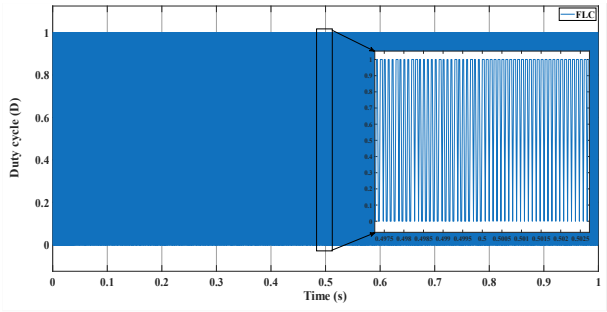

Figure 28. Duty-cycle control signal for Fuzzy Logic Controller (FLC) case 3

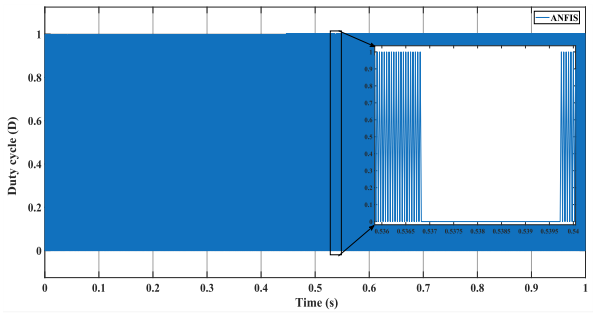

Figure 29. Duty-cycle control signal for adaptive neuro-fuzzy inference system (ANFIS) case 3

Table 4. Dynamic parameter

		Transient Parameter		
Case	**Controller**	**Rise time (t_r)**	**Settling Time (t_s)**	**Max Overshoot (M_p) %**
Case 1	PID	0.041	0.194	20.94
	FLC	0.04	0.053	4.6
	ANFIS	0.04	0.039	1.92
Case 2	PID	0.60225	0.57	NAN
	FLC	0.622	0.601	0.5695
	ANFIS	0.5196	0.5272	1.795
Case 3	PID	0.5368	0.6747	13.956
	FLC	0.5369	0.5348	1.924
	ANFIS	0.5369	0.5349	0.562

Table 5. Performance parameter

		Transient Parameter		
Case	**Controller**	**RMSE**	**MAE**	**ITAE**
Case 1	PID	0.6231	0.1676	0.008686
	FLC	0.5851	0.1193	0.01091
	ANFIS	0.5844	0.1041	0.003924
Case 2	PID	0.8707	0.3293	0.0537
	FLC	0.8188	0.2355	0.05027
	ANFIS	0.783	0.1727	0.01649
Case 3	PID	0.6697	0.243	0.05067
	FLC	0.615	0.1509	0.02716
	ANFIS	0.6147	0.1359	0.02032

The Neuro-Fuzzy Controller (ANFIS) exhibited the most desirable transient characteristics in every dynamic test, both with reference steps and with load perturbations, and had the shortest settling time, with virtually no steady-state error. The FLC was also competitive in terms of speed, as it arrived at the final value with minimal residual oscillations. Compared with the other controllers, the PID controller had the weakest disturbance-rejection capabilities, with larger transient excursions and slower recovery. The general performance is thus ranked as: ANFIS > FLC > PID.

5. CONCLUSIONS

This paper compared PID, FLC, and an ANFIS-based neuro-fuzzy controller for output-voltage regulation of a DC–DC buck converter under identical reference-step and load-disturbance scenarios. The observed trends align with fundamental control principles. PID offers linear fixed-gain compensation: integral action removes steady-state error, and derivative action enhances damping, but constant gains limit adaptability when the plant's dynamics change. FLC implements a nonlinear mapping from (e, e′) to the duty-cycle command that effectively performs gain scheduling—delivering strong correction for large deviations and gentler action near regulation—thus improving damping and reducing ripple. ANFIS extends this ability by training its premise membership functions and consequent coefficients, resulting in smoother interpolation and locally adjusted surface slopes that boost disturbance rejection and transient recovery. From a practical standpoint, PID is suitable for low-cost implementations with moderate performance needs and a narrow operating range. FLC is beneficial when an accurate model isn't available and moderate complexity is acceptable; it can be designed from expert knowledge and remains understandable. ANFIS is recommended for performance-critical regulation, but it requires representative training data, extra computation, and explicit checks for generalization across operating conditions. These trade-offs directly influence controller choice in real-world buck-converter applications. This study is limited to simulation with nominal parameters. Parameter uncertainties and converter non-idealities (e.g., ESR, quantization, sensor noise, and computation delay) were not systematically examined, and no hardware prototype validation was performed. Additionally, the comparative study considers only a single nominal converter design; broader operating ranges and uncertainty analyses will be explored in future work.

This study can be enhanced by incorporating artificial intelligence (AI) to improve the performance of voltage regulation [16-21]. Moreover, other control techniques can be suggested to compare to the proposed controller in this study [22-30].

REFERENCES

[1] Al-dalawi, R.M., Al-Dujaili, A., Pereira, D.A. (2023). A comprehensive review of multi-port DC/DC converters for the off-grid system integration with renewable energy resources. Journal of Techniques, 5(2): 61-73. https://doi.org/10.51173/jt.v5i2.1227

[2] Ding, X., Chan, P.K., Leung, K.N. (2020). A 40 nm CMOS hysteretic buck DC-DC converter with digital-controlled power-driving-tracked-duration current pump. IEEE Access, 8: 177374-177384. https://doi.org/10.1109/ACCESS.2020.3026678

[3] Yusoff, M.J., Ismail, N.N., Musirin, I., Hashim, N., Johari, D. (2010). Comparative study of fuzzy logic controller and proportional integral derivative controller on dc-dc buck converter. In 2010 4th International Power Engineering and Optimization Conference (PEOCO), pp.

142-148. https://doi.org/10.1109/PEOCO.2010.5559170
[4] Swathy, K., Jantre, S., Jadhav, Y., Labde, S.M., Kadam, P. (2018). Design and hardware implementation of closed loop buck converter using fuzzy logic controller. In 2018 Second International Conference on Electronics, Communication and Aerospace Technology (ICECA), Coimbatore, India, pp. 175-180. https://doi.org/10.1109/ICECA.2018.8474570
[5] Fudoli, F.H., Vechia, D.D., Bonaldo, J.P., Bertogna, E.G. (2018). Design, simulation and comparative evaluation of both a classic and a fuzzy logic PI controller applied to a DC-DC converter. Przeglad Elektrotechniczny, 94(5): 27-31. https://doi.org/10.15199/48.2018.05.05
[6] Guiza, D., Soufi, Y., Ounnas, D., Metatla, A. (2019). Design and implementation of takagi-sugeno fuzzy tracking control for a dc-dc buck converter. Advances in Electrical and Electronic Engineering, 17(3): 234-243. 10.15598/aeee.v17i3.3126
[7] Bhat, N.D., Kanse, D.B., Patil, S.D., Pawar, S.D. (2020). DC/DC buck converter using fuzzy logic controller. In 2020 5th International Conference on Communication and Electronics Systems (ICCES), Coimbatore, India, pp. 182-187. https://doi.org/10.1109/ICCES48766.2020.9138084
[8] Martínez, F., Montiel, H., Martínez, F. (2023). Fuzzy control of synchronous buck converters utilizing fuzzy inference system for renewable energy applications. International Journal of Electrical & Computer Engineering, 13(5): 5076-5090. https://doi.org/10.11591/ijece.v13i5.pp5076-5090
[9] Shaikh, U.A., AlGhamdi, M.K., AlZaher, H.A. (2018). Novel product ANFIS‐PID hybrid controller for buck converters. The Journal of Engineering, 2018(8): 730-734. https://doi.org/10.1049/joe.2018.0113
[10] Shabaninia, F., Pouyanfar, S., Abbasi, S.H. (2014). Design and analysis of neuro fuzzy logic PD controller for PWM-based switching converter. Universal Journal of Control and Automation, 2(2): 58-64.
[11] Nejad, M.B., Ghamari, S.M., Mollaee, H. (2023). Adaptive neuro‐fuzzy inference systems controller design on Buck converter. The Journal of Engineering, 2023(10): e12316. https://doi.org/10.1049/tje2.12316
[12] Aldalawi, R., Al-Dujaili, A., Pereira, D. (2024). Robust adaptive control for the DC-DC converter in the presence of parametric uncertainty. AIP Conference Proceedings, 3232(1): 030009. https://doi.org/10.1063/5.0236921
[13] Shanmugasundaram, R., Ganesh, C., Singaravelan, A., Gunapriya, B., Adhavan, B. (2021). High-performance ANFIS-based controller for BLDC motor drive. In Ubiquitous Intelligent Systems: Proceedings of ICUIS 2021, pp. 435-449. https://doi.org/10.1007/978-981-16-3675-2_33
[14] Coteli, R., Acikgoz, H., Ucar, F., Dandil, B. (2017). Design and implementation of Type-2 fuzzy neural system controller for PWM rectifiers. International Journal of Hydrogen Energy, 42(32): 20759-20771. https://doi.org/10.1016/j.ijhydene.2017.07.032
[15] Çöteli, R., Açikgöz, H., DANDIL, B., Tuncer, S. (2018). Real-time implementation of three-level inverter-based D-STATCOM using neuro-fuzzy controller. Turkish Journal of Electrical Engineering and Computer Sciences, 26(4): 2088-2103. https://doi.org/10.3906/elk-1708-281
[16] Shahid, M.A., Abbas, G., Hussain, M.R., Asad, M.U., et al. (2019). Artificial intelligence-based controller for DC-DC flyback converter. Applied Sciences, 9(23): 5108. https://doi.org/10.3390/app9235108
[17] Faraj, H.Z., AL-Dujaili, A.Q., Humaidi, A.J. (2023). The classification method of electrical faults in permanent magnet synchronous motor based on deep learning. In 2023 IEEE 11th Conference on Systems, Process & Control (ICSPC), Malacca, Malaysia, pp. 326-331. https://doi.org/10.1109/ICSPC59664.2023.10420154
[18] Mohammed, H., Ibrahim, M., Raoof, A., Jaleel, A., Al-Dujaili, A.Q. (2025). Modified ant colony optimization to improve energy consumption of cruiser boundary tour with internet of underwater things. Computers, 14(2): 74. 1https://doi.org/10.3390/computers14020074
[19] Ziad, H., Al-Dujaili, A., Humaidi, A. (2024). Techniques used in faults detection of permanent magnet synchronous motor: A review. AIP Conference Proceedings, 3232(1): 030004. https://doi.org/10.1063/5.0236292
[20] Ziad, H., Al-Dujaili, A.Q., Humaidi, A.J. (2025). A comparative study of deep learning efficiency in the classification of electrical faults of permanent magnet synchronous motor. International Review of Applied Sciences and Engineering, 16(2): 292-302. https://doi.org/10.1556/1848.2024.00885
[21] Abdulhadi, J., Al-Dujaili, A., Humaidi, A.J., Fadhel, M.A.R. (2021). Human nail diseases classification based on transfer learning. ICIC Express Lett, 15(12): 1271-1282. https://doi.org/10.24507/icicel.15.12.1271
[22] Hadi, Z.G., Ajel, A.R., Al-Dujaili, A.Q. (2021). Comparison between CNN and SVM in skin cancer images recognition. Journal of Techniques, 3(4): 15-22. https://doi.org/10.51173/jt.v3i4.390
[23] Al-Dujaili, A.Q., Humaidi, A.J., Allawi, Z.T., Sadiq, M.E. (2023). Earthquake hazard mitigation for uncertain building systems based on adaptive synergetic control. Applied System Innovation, 6(2): 34. https://doi.org/10.3390/asi6020034
[24] Husain, S.S., Al-Dujaili, A.Q., Jaber, A.A., Humaidi, A.J., Al-Azzawi, R.S. (2024). Design of a robust controller based on barrier function for vehicle steer-by-wire systems. World Electric Vehicle Journal, 15(1): 17. https://doi.org/10.3390/wevj15010017
[25] Hasan, A.F., Al-Shamaa, N., Husain, S.S., Humaidi, A.J., Al-dujaili, A. (2024). Spotted hyena optimizer enhances the performance of fractional-order PD controller for tri-copter drone. International Review of Applied Sciences and Engineering, 15(1): 82-94. https://doi.org/10.1556/1848.2023.00659
[26] Humaidi, A.J., Hameed, M.R., Hasan, A.F., Al-Obaidi, A.S.M., et al. (2023). Algorithmic design of block backstepping motion and stabilization control for segway mobile robot. In Mobile Robot: Motion Control and Path Planning, pp. 557-607. https://doi.org/10.1007/978-3-031-26564-8_16
[27] Ziad, H., Al-dujaili, A., Humaidi, A.J. (2024). Electrical faults classification in permanent magnet synchronous motor using ResNet neural network. International Review of Applied Sciences and Engineering, 15(3): 355-364. https://doi.org/10.1556/1848.2024.00789
[28] Al-Dujaili, A., Cocquempot, V., Najjar, M.E.E., Pereira, D., Humaidi, A. (2023). Fault diagnosis and fault tolerant control for-linked two wheel drive mobile robots. In Mobile Robot: Motion Control and Path Planning, pp.

403-437. https://doi.org/10.1007/978-3-031-26564-8_13
[29] Al-Dujaili, A., Cocquempot, V., Najjar, M.E.B.E., Pereira, D., Humaidi, A. (2023). Adaptive fault-tolerant control design for multi-linked two-wheel drive mobile robots. In Mobile Robot: Motion Control and Path Planning, pp. 283-329. https://doi.org/10.1007/978-3-031-26564-8_10
[30] Hameed, A.M., Al-Dujaili, A., Humaidi, A.J. (2025). Fuzzy logic control-based battery management system. International Review of Applied Sciences and Engineering, 16(3): 437-452. https://doi.org/10.1556/1848.2025.00971
[31] AL-Hashemi, S.A., Ayad, A.D., Ajel, A.R. (2021). Speed control using an integral sliding mode controller for a three-phase induction motor. Journal of Techniques, 3(3): 10-19. https://doi.org/10.51173/jt.v3i3.328

NOMENCLATURE

Vin	Input voltage of the buck converter
Vo	Output voltage of the buck converter
Vref	Reference output voltage
iL	Inductor current
L	Inductance
C	Capacitance
R	Load resistance
d	Duty cycle
D	Duty-cycle command
ΔD	Duty-cycle increment
e(t)	Voltage tracking error
e′(t)	Derivative of tracking error
fs	Switching frequency
Kp, Ki, Kd	PID controller gains
tr	Rise time
ts	Settling time
Mp	Maximum overshoot

Greek symbols

ωc	Gain crossover frequency
ωzi	Integral zero frequency
ωzd	Derivative zero frequency
μ(.)	Membership function degree

Subscripts

in	Input
o	Output
ref	Reference value
L	Inductor-related variable
i	Rule or index number
k	Sample index
PID	Proportional–Integral–Derivative
FLC	Fuzzy Logic Controller
ANFIS	Adaptive Neuro-Fuzzy Inference System

APPENDIX

TableA1. Training data of ANFIS

e	Δe	D
0.098343095	-0.272462138	-0.00379
0.773483295	-0.276801137	0.063508
-0.785743835	-0.484586626	-0.1028
-0.53426257	0.26735016	-0.04006
-0.962734568	0.01245631	-0.09565
0.69445012	-0.396012848	0.049644
-0.831368953	0.276483574	-0.06931
0.733293477	-0.339835375	0.056338
0.853059515	0.401729029	0.105392
0.982013264	0.255716221	0.110987
0.798317315	0.050224603	0.082343
0.68413502	0.030578233	0.069942
-0.824044257	-0.199040686	-0.09236
-0.135888071	-0.486926353	-0.03794
-0.342379865	-0.04263366	-0.03637
-0.288708883	-0.357191455	-0.04673
-0.920774901	0.093379357	-0.08741
-0.339708764	0.329763045	-0.01748
0.84384454	-0.114309198	0.078669
0.708376167	-0.218837412	0.059896
-0.537965413	-0.329006877	-0.07025
-0.648056465	-0.478096003	-0.08871
-0.725762646	-0.271635448	-0.08616
0.304289284	0.280748129	0.044466
-0.932091288	0.402305865	-0.07309
-0.113082245	0.14290556	-0.00416
0.161790077	-0.296568221	0.001351
0.764583304	-0.184765529	0.06722
-0.744356246	0.314498736	-0.05871
-0.397757283	-0.47844468	-0.0637
0.353884371	0.322389861	0.051508
0.656562265	0.447760748	0.088044
-0.526135254	0.008082383	-0.05221
0.151681121	0.161307623	0.023233
0.533067705	-0.436328167	0.03149
0.702438094	-0.385494279	0.050969
0.046106091	0.307406427	0.019981
0.819973358	-0.456209537	0.059187
-0.45837156	-0.31226064	-0.06145
0.039845427	-0.231432895	-0.00759
0.969138253	0.203140282	0.107071
-0.61116526	0.034627903	-0.05939
0.118552337	0.341679979	0.028939
-0.067863831	0.283549667	0.007391
0.515259263	-0.053010696	0.048875
0.305729199	0.020844153	0.031615
0.513632214	0.253274658	0.064027
-0.412207517	-0.374668096	-0.05995
0.718221343	0.46580594	0.095112
-0.250346115	0.04082357	-0.02299
-0.302802932	-0.426341313	-0.0516
-0.613469722	0.430470232	-0.03982
-0.29416267	0.405310285	-0.00915
0.435945551	0.314811679	0.059335
0.333157671	0.387144589	0.052673
-0.230088797	-0.414940204	-0.04376
-0.376974928	-0.463078424	-0.06085
0.557919217	0.066935085	0.059139
0.609267028	-0.422967978	0.039778
0.732435534	0.137632727	0.080125
0.885542804	0.308344833	0.103972
-0.228445661	0.481724872	0.001242
-0.230832811	-0.158105354	-0.03099
0.106444677	0.10852937	0.016071
0.625558628	0.245552873	0.074834

0.691492151	-0.293783273	0.05446
0.253261311	0.139573527	0.032305
-0.748666501	-0.287537572	-0.08924
-0.089569922	-0.078125023	-0.01286
0.757485364	-0.077573104	0.07187
-0.723330198	-0.446975066	-0.09468
0.578181844	0.255282285	0.070582
0.333564845	0.091629644	0.037938
-0.250375085	-0.264570318	-0.03827
-0.206604302	-0.267014412	-0.03401
-0.987020175	-0.44095135	-0.12075
-0.827491606	-0.228810966	-0.09419
-0.669944123	-0.047788998	-0.06938
0.916538458	0.145292712	0.098918
-0.20394154	0.327549863	-0.00402
0.594594577	0.304582772	0.074689
-0.534690403	0.052849171	-0.05083
0.517810261	-0.370526501	0.033255

0.115095918	-0.350854252	-0.00603
-0.271235127	0.09358388	-0.02244
-0.459630133	0.038137828	-0.04406
-0.622910546	-0.300157275	-0.0773
0.703950422	-0.499543004	0.045418
-0.752311938	-0.21883094	-0.08617
-0.56678437	-0.031910938	-0.05827
-0.515379978	-0.319870247	-0.06753
0.189952509	-0.363349567	0.000828
0.727112846	-0.148626205	0.06528
-0.810370173	-0.199209543	-0.091
0.250943946	-0.193378045	0.015425
0.760920471	-0.207726451	0.065706
0.571750687	-0.485950353	0.032878
-0.498399241	-0.408854801	-0.07028
0.309753924	-0.233493298	0.019301
0.564587588	0.22133447	0.067525